

Object Models in Multiscale Intrinsic Coordinates via M-reps

Stephen M. Pizer, P. Thomas Fletcher, Andrew Thall,
 Martin Styner, Guido Gerig, Sarang Joshi
 Medical Image Display & Analysis Group, University of North Carolina, Chapel Hill, USA
 Email: pizer@cs.unc.edu

Abstract -- Object descriptions used for 3D segmentation by deformable models and for statistical characterization of 3D object classes benefit from having intrinsic correspondences over deformation of the objects or multiple instances in the same object class. These correspondences apply over a variety of spatial scale levels and consequently lead to efficient segmentation and probability distributions of geometry that are trainable with an achievable number of training instances. This paper describes a figural coordinate system provided by m-reps models and shows how such coordinates not only provide the required positional correspondences, but also are intuitive and provide orientational and metric correspondences. Examples are given for the segmentation of kidneys from CT and for the statistical characterization of schizophrenia and control classes of cerebral ventricles and of hippocampus pairs.

I. INTRODUCTION

Consider the kidney bean object. Describing the relation between one bean and another requires that the tip of one bean correspond to the tip of another, that the middle of the crest along the backbone of one bean correspond to that position on another, etc. Moreover, moving along the bean requires following the curve of the bean, giving an orientational correspondence at corresponding positions of the two beans, even if one is straighter than the other. The same is true in moving across the bean from the crest on the convex curve to the crest on the concave curve of the bean. Said another way, we discuss kidney beans best in an intrinsic kidney bean coordinate system. In this coordinate system, one of the coordinates should progress from one end of the bean to the other. Another coordinate should progress from the convex crest to the concave crest. A third coordinate would progress from one of the flattish sides of the bean to the other.

The same argument applies for the fleshy main part of the hand with the palm on one of its sides and the apparent blood vessels on the other side, but it applies also for each of the fingers, except that the fingers have the special property of being attached to the main part of the hand, and moving from the attachment end to a fingertip end provides one the intrinsic coordinate directions desired. That is, we require a uniform coordinate system for the whole hand, describing not only the six individual parts ("figures") just discussed but also how we pass from one part to another in the attachment region. This coordinate system needs to apply to the inside of the hand, the surface of the hand, and the region near to and outside the hand.

What we have described is handled mathematically via a medial representation, because it provides both the subdivision into parts and the crest-to-crest, end-to-end, and cross-figural coordinates that we have sketched. We refer to

such an object description so represented as an *m-rep*. The *m-rep* for an object consists of a discrete collection of interrelated medial sheets, and we call the part of the object associated with a particular sheet a *figure*. We refer to the whole object-intrinsic coordinate system we are describing as the *figural coordinate system* of an object. From our point of view these medial sheets form a component of the object description that is primitive, i.e., not derived from other descriptors such as the boundary. The correspondences across two conformations of an object obtained by having the same figural coordinates (Fig. 2) are helpful to relate deformable models in segmentation and to designate homologous points in statistical geometric description of a class of objects. Because these intrinsic coordinate systems provide the homology on which such statistical descriptions of geometry of populations must depend and because sampling from the resulting populations of *m-reps* yields a generated object from which both the internal space and the boundary can be produced and locally described, these *m-reps* based coordinates provide an effective means of generative object modeling.

The focus of this paper and its new material are the detailing of the figural coordinates provided by *m-reps* and evidence of the usefulness of the correspondences provided by these object-intrinsic coordinates. *M-reps* themselves have been described elsewhere [Pizer 2002, Fletcher 2002], and the particular applications in segmentation and statistical characterization that are given here have also been reported recently in other papers, though not in regard to providing evidence in regard to the usefulness of the intrinsic coordinates that they provide.

In section II we will focus on intrinsic coordinates for single-figure objects, those that are represented with a single medial sheet. This representation will also apply for the individual figures making up multifigure objects. Section III will then focus on intrinsic coordinates for multifigure objects, with an emphasis on the region where one figure, a *subfigure*, blends into a parent figure. We will also there face the issue of the relationship of neighboring, unattached figures, such as adjacent fingers in a hand.

Section IV will face the notion of multiscale coordinate systems. Such coordinates not only integrate, for example, the figural coordinate systems with the object coordinate system but also allow a coarse-to-fine succession of representations for a single figure as well as a fine scale (or set of scales) of representations of the boundary detail. In that section we will explain why a representation with many scale levels is necessary for both 3D segmentation by deformable models and statistical geometric characterization of 3D object classes. Section V will give example results from each of these classes of driving problem, with special focus on the usefulness of

intrinsic correspondences in these problems. In deformable model segmentation the correspondence goes across deformation and affects both the geometric typicality term of the objective function being optimized in deformable model segmentation and the term measuring the match of the target image against model-relative templates. In statistical geometric characterization the correspondence forms the homology between instances of the population. Section VI will close the paper with the relation of our figural coordinate system to other intrinsic coordinate systems and other discussion and conclusions.

II. SINGLE-FIGURE INTRINSIC COORDINATES BASED ON M-REPS

While m-reps have been described in detail elsewhere, they provide the foundation for the intrinsic coordinate system that is the main subject of this paper, so we briefly describe them here. An m-rep for a generic figure in our system is a 2-manifold of medial atoms (Fig. 1), where an interior medial atom is a medial position at which two vectors (called *port* and *starboard sails*) of equal length r share a tail and where a mesh-edge medial atom in addition is equipped with a bisector vector of the two sails of length greater or equal to the common sail length. This medial representation implies (as opposed to being implied by) a boundary that is incident to and orthogonal to the sail tips for each sail and at the bisector vector tip. The locus of bisector tips for sheet-edge medial atoms forms the crest cycling the boundary of the figure. The two coordinates along and across the manifold provide the along-figural parametrization that is needed, and the along-sail directions provide the cross-figural coordinate. In the examples shown here the medial manifold is sampled into a quad-mesh, but the sampling issues will not be emphasized in this paper.

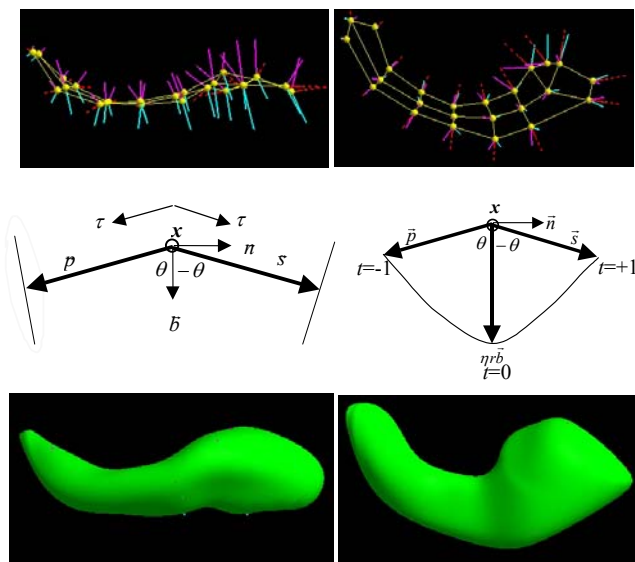


Fig. 1. Top: an m-rep for a hippocampus, viewed from two directions. Each ball with two line segment sails forms a medial atom. Shown are a quad-mesh of samples of the continuous 2-manifold of medial atoms. Center: an internal medial atom and a sheet-edge medial atom, each with their implied boundaries. Bottom: The boundary implied by the m-rep, viewed from the two directions.

We will denote by (u,v) the coordinates along the medial manifold. These coordinates can be visualized as moving on the positional locus forming the skeleton of the figure. For single figures we will arbitrarily visualize v as describing the most elongated direction of the manifold, and for subfigures we will let v describe the direction away from the end of the manifold that is attached to the parent figure. Realizing that the crest is geometrically special, we will denote by t the coordinate that describes the side of the figure corresponding to either the starboard sails ($t=+1$) or the port sails ($t=-1$) and that takes one around the crest (at $t=0$) by passing from $t=-1$ continuously to $t=+1$. The final coordinate, measuring distance along the sail directions will be denoted by τ . In order to allow the inside of the figure to be easily distinguished from the outside, we will place the origin for τ to be at the medially implied figural boundary. That is, $\tau < 0$ in the interior of the figure, and $\tau > 0$ in the exterior of the figure. Points on the medially implied boundary, where $\tau=0$, are described the coordinates (u,v,t) . Each boundary point thereby carries a normal in the direction of the sail abutting there, two linearly independent directions in the tangent plane to the boundary corresponding to moving in the figural u and v coordinates respectively, and a ruler $r(u,v)$.

For the (u,v,t,τ) coordinate system to be locally useful for shape description and thus be locally similarity transform invariant, all distances must scale proportionally. Since the medial width r is the basic distance for a medial atom, the u,v coordinate pair must be set up so that geodesic distances along the skeleton are in r -proportional units. Similarly, distances along the sails, i.e., along τ , must be in r -proportional units. This leads to the natural situation of $\tau=-1$ at the skeleton and of $|\tau|$ in the interior measuring the proportion of the way in from the medially implied boundary to the skeleton.

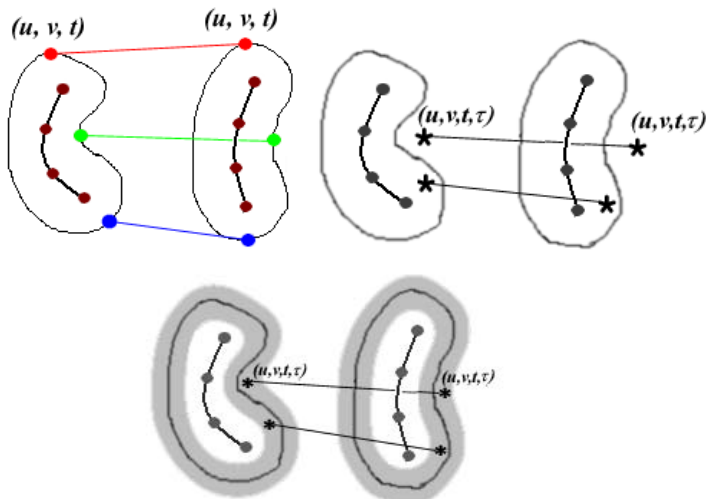


Fig. 2. Medially implied correspondences between a typical figure and a deformed figure for figural boundary positions (leftmost), for positions interior and exterior to the boundary (center), and for the boundary collar (right), which is particularly relevant for intensity correspondences between a template image and a target image.

M-reps provide orientation correspondence as well as positional and metric correspondence. By metric correspondence we mean that at corresponding positions in two instances of an object there is a homology between distances from that point in one object with distances from the corresponding point in the other object. By orientation correspondence we mean the homology at the corresponding positions between directions from that point in one object and directions from the corresponding point. For example, the direction along one kidney bean from one point inside the bean should correspond to the direction along another kidney bean at the corresponding internal position. Along the medial sheet, and by implication at all locations (u,v,t,τ) with the same (u,v,t) , this correspondence is provided by the ∇r direction, which bisects the sails, as well as by the orthogonal direction on the medial locus tangent plane and the sail direction on the side of the medial sheet given by t .

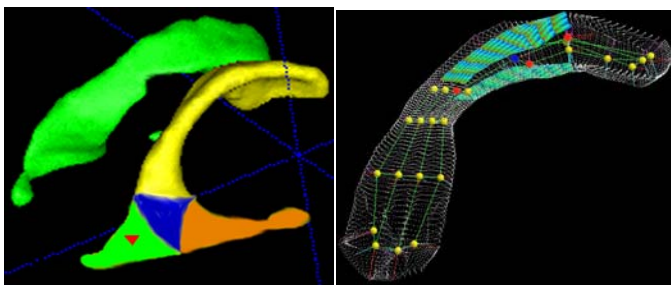


Fig.3. Multiscale levels for the cerebral ventricles. Left, all colored items: the object complex level, describing two related lateral ventricles. At the object level, a right lateral ventricle is made up of 4 separately colored figures. Those figures are the temporal, occipital, and lateral horns and the atrium of the ventricle. Right: the figural section level, describing a through section of a figure, here the lateral horn. The triangle in the left figure is at the boundary level, describing detail on the boundary via tiling.

Besides providing the needed correspondences, the figural coordinate system has the following advantages for representing objects involved in deformable model segmentation or shape characterization.

1. Each medial atom represents an interior section of a figure, leading to a special capability for deformation of the interior.
2. In medicine, our main application, since figures typically have anatomic names and each medial atom in the m-rep corresponds to an interior slab of the figure bounded by its immediately neighboring medial atoms, the geometric transformations involved in the deformation can be described with medical relevance and with appropriate locality. This property of there being intuitive, already named figures also holds in other applications.
3. An m-rep lends itself directly to representation at multiple scale levels. There are additional important scale levels besides those already mentioned (object, figure, boundary). For objects consisting of more than one figure or for sets of objects [Fletcher 2000], situations not described in this paper, there are the larger scale multi-object and object scale levels. Also described elsewhere [Yushkevich 2001], there are opportunities for multiple levels of meshing of each figure, with each mesh element

corresponding to a figural section, i.e., a through-section of the figure capturing the region centered at a particular mesh medial atom and bounded by its neighboring mesh atoms (see Fig 3).

III. INTRINSIC COORDINATES IN MULTIFIGURE OBJECTS

Positions near or inside the figures making up a multifigure object are parameterized effectively in an object-intrinsic fashion by a label indicating which figure is the near one and the (u,v,t,τ) coordinates relative to that figure. In the region where a subfigure joins a parent figure, a different solution is necessary. Whereas Blum (1978) described subfigures via a branching skeleton, the point of view that we have taken, in which a medial atom is a primitive that covers an infinitesimal section of the object interior, leads to seeing a subfigure as riding on the medially implied boundary of the parent figure. In this view every end coordinate of the subfigure that is on this “hinge” with the parent figure can be known by the figural coordinate (u,v,t) of the parent’s boundary point at which it is located and the orientation of the parent’s figural coordinate system there. The effect is that as the parent figure deforms, the location and normal of the point with the hinge (u,v,t) changes and so correspondingly does the atom at the subfigure end, and as a result the whole subfigure can translate, rotate, scale, and deform accordingly.

But the subfigure will frequently meet the parent figure along a smooth boundary rather than forming an intersection with a sharp corner (see Fig. 4). In this blending region, including parts of space nearest to this blend region we need a new coordinate system. Two of these coordinates, namely the u and t coordinates of the subfigure, will take us around the subfigure. Another coordinate, which we denote by w , is needed to pass from the subfigure to the parent figure. A final coordinate, again τ , is needed to measure an extension of the idea of r -proportional distance into the interfigural blend region. Thus the figural coordinate system in the region of the interfigural blend is (u,w,t,τ) , where u and t are the same object intrinsic coordinates as that of subfigure and w and τ have to appropriately blend the coordinates of the parent figure and the subfigure.

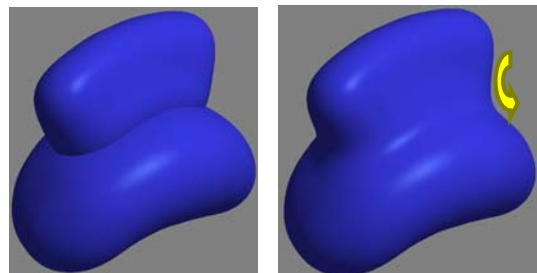


Fig.4. Left: the vertical subfigure has a sharp corner with its parent figure (the smoothness parameter $s=0$). Right: the vertical figure has a smooth transition into its parent figure ($s>0$).

The coordinate w needs to measure the comparative distance between the parent figure, which we will call figure 1, and the subfigure, which we will call figure 2. Since τ_1

measures the figural distance to the parent figure and τ_2 measures the figural distance to the subfigure, w should be proportional to $\tau_2 - \tau_1$. i.e., $w = (\tau_2 - \tau_1)/T$. Let the normalizing distance T be the figural distance at which we switch from a blended hinge-region distance τ_{12} to the ordinary figural distance τ_1 or τ_2 , respectively. Thus the blend region is defined as $|w| < 1$, with $w = -1$ on the subfigure side (at the subfigure boundary $\tau_1 = T$ and $\tau_2 = 0$) and $w = +1$ on the parent figure side (at the parent figure boundary $\tau_1 = 0$ and $\tau_2 = T$). The blend must be computed along w from $(u, -1, t, \tau_2)$ to $(u, +1, t, \tau_1)$ for each u, t pair. A parameter s can control the smoothness of the transition.

We have achieved this blending and the computation of figural distances in two alternative ways: by interpolating blended distance τ_{12} from the values of τ_1 and τ_2 and then defining the boundary implicitly as the zero of this distance [Pizer 2002], and by using an interpolating variant of subdivision surfaces to connect the discrete boundary tiles formed from the m -rep of the individual figures [Thall 2002].

Points inside the figure and outside it but inside the caustic (focal) surface can also be put into correspondence in a figurally relative manner. Correspondences outside the caustic surface have also been defined via external medial loci and thus between separated object, between separated subfigures in an object, or between distant parts of a figure with concave boundary [Crouch 2001]. Such external correspondences can also involve measuring distances in a way reflecting convexification of the boundary by scale-based averaging in proportion to the point's distance from that boundary. However, these issues are beyond the scope of this paper. These external correspondences can be used to describe the relation of the boundary of one figure with another and thus to prevent penetration between separated figures during deformation, as well as to separately measure the distance between the boundary of one figure and another and the distance of sliding of one object along another [Fletcher 2002].

IV. INTRINSIC OBJECT COORDINATES AT MULTIPLE SCALE LEVELS

We desire successful segmentation performance that is linear in the number of the smallest scale geometric primitives, for example the boundary tiles defining the segmented object's surface or the voxels making up the object. We desire statistical description of object geometry that can be stably trained with a limited (e.g., some tens) of training instances. A description with multiple scale levels can achieve these objectives. Multiscale descriptions do so by representing geometric primitives at one scale level with neighbor relationships appropriate for that scale level and thus at distances roughly proportional to the scale and in relation to their parent geometric primitives at the next larger scale. Relationships between primitives at one scale and nearby ones at adjacent scales are also needed, and typically the relationship is taken to represent residues describing the description at one scale and at the collection of larger scales [Yushkevich 2001]. That is, figural coordinates undergo

residue offsets (diffeomorphisms) from their values at the next larger scale.

In our method the scale levels are object-intrinsic. That is, the levels are [1] the object complex scale level, [2] the object scale level, [3, 3a, 3b, ...] the figural scale levels, [4, 4a, 4b, ...] the medial atom or figural section scale levels, [5, 5a, 5b, ...] the boundary atom scale levels, and [6] the voxel scale level. At all level numbers < 5 the objects are represented by medial atoms, at level 5, 5a, etc. these are augmented by boundary atoms, and at level 6 places in space are represented by a field of offsets specifying a further diffeomorphism.

Figural coordinates are defined with respect to a scale level and are produced by successive residues from the largest scale level to the scale level in question.

V. INTRINSIC COORDINATES IN SEGMENTATION BY DEFORMABLE MODELS AND STATISTICAL OBJECT CLASS CHARACTERIZATION

Deformable model segmentation proceeds by a series of stages producing deformations of a geometric model to optimize an objective function. At each stage the objective function reflects the match of the model to the target image, and the algorithm involves either constraints on the deformation or a term in the objective function measuring the geometric typicality of the deformed object. Measuring both the model to image match and geometric typicality requires positional correspondences that are well provided by intrinsic coordinates.

Statistical object class characterization produces a description of the geometry of the population of objects in each class and the differences between classes. For example, the differences in the shape of the hippocampus pair between schizophrenic and control classes can give indications of the biological changes associated with the development of schizophrenia. Describing the geometric properties of the population of objects in a class requires correspondence of positions between objects in the same class and possibly between objects in a single person, e.g., between the left and right hippocampi. Describing the interclass differences requires correspondence of positions of objects in different classes. These correspondences are well provided by equality of intrinsic coordinate values.

These two uses of intrinsic coordinates are described below, in sections V.A and V.B, respectively, with illustrations of the success of the resulting methods.

A. Segmentation by deformable m -rep models via intrinsic coordinates

We summarize the deformable m -rep 3D segmentation method, described in detail elsewhere [Pizer 2002]. In doing so, we emphasize the use of the object-intrinsic coordinates.

The deformable m -reps method operates from large to small scale levels, at each level k deforming the represented object \underline{m} by optimizing an objective function $F_k(\underline{m}, I_{\text{target}})$ over the set of geometric transformations available at that scale level. As with many deformable model based

segmentation methods, each objective function F_k is the sum of two terms, one measuring the geometric typicality of $\underline{\mathbf{m}}$ and the other measuring the match of $\underline{\mathbf{m}}$ to the target image I_{target} . At each stage of the algorithm the geometric typicality is the negative of the deviation from the deformed model that is the result of the previous stage. With figural intrinsic coordinates this can be measured for any position with figural coordinates (u, v, t, τ) (or (u, w, t, τ) for interfigural blend regions) by the negative of the Euclidean distance between that point in the model and that point in the deformed model (Fig.2), in units of the local ruler, i.e. scaled by the r value associated with the model point (u, v, t, τ) . In our method the square of this distance is averaged over the boundary points (i.e., $\tau = 0$) of the figure, group of figures, atom-related figural section, or boundary section associated with the geometric primitive being optimized. This mean is measured between the version of the deformed model produced at the next larger level of scale and the newly deformed candidate $\underline{\mathbf{m}}$.

As is common, the match of $\underline{\mathbf{m}}$ to the target image is measured in a region near the object boundary that we call a boundary *collar* (Fig. 2). $\underline{\mathbf{m}}$ is matched to I_{target} at collar positions with the same intrinsic coordinates (u, v, t, τ) (or (u, w, t, τ) for interfigural blend regions), before and after deformation of the model into $\underline{\mathbf{m}}$. The template image is defined on the model. The template can be an ideal image, e.g., defined by directional derivatives of a Gaussian, or it can be the training image from which the model was built, or it can be based on the statistics of a set of training images from which the model was built. In all three cases the template width varies with collar boundary position in proportion to the associated r , and in the latter two cases the template benefits from having a different functional profile at different boundary positions. In our method the template to target image match is computed via normalized correlation with an equally spaced sampling of τ between $-k$ and $+k$ ($k = 0.33$ is a typical value), but other measures of template match, such as normalized mutual information are possible [Willis 2001]. We have implemented such a training image template for collars of half-width $r/3$.

The algorithm presently begins with a manual placement the model in the 3D image, thereby choosing a similarity transform. The initial models $\underline{\mathbf{m}}_0$ used in this work (Figs. 1 & 5) were developed by automatic analysis of the geometry of a training set of hand segmented instances of the object over a variety of patients [Styner 2001a] or by manual construction on a single training image according to set of rules determined by the mathematics of medial geometry [Damon 2002].

We have tested this method for the extraction of three anatomic objects well modeled by a single figure: the lateral cerebral ventricle, the kidney parenchyma + pelvis, and the hippocampus. Results of a kidney segmentation are visualized in Fig. 5. For 24 kidneys we were able to extract the kidney with a median accuracy of boundary position of < 1 voxel as compared to human manual segmentations. More results can be found on the webpage midag.cs.unc.edu/projects/defmreps. We ascribe the good quality of these results to three factors: 1) the multiple scale level approach with geometric typicality at each stage depending on the result of the previous stage, 2) the ability of

the m-rep representation to provide object-intrinsic correspondences at the figural and figural section stages, 3) the availability of the training intensity template for the more difficult cases.

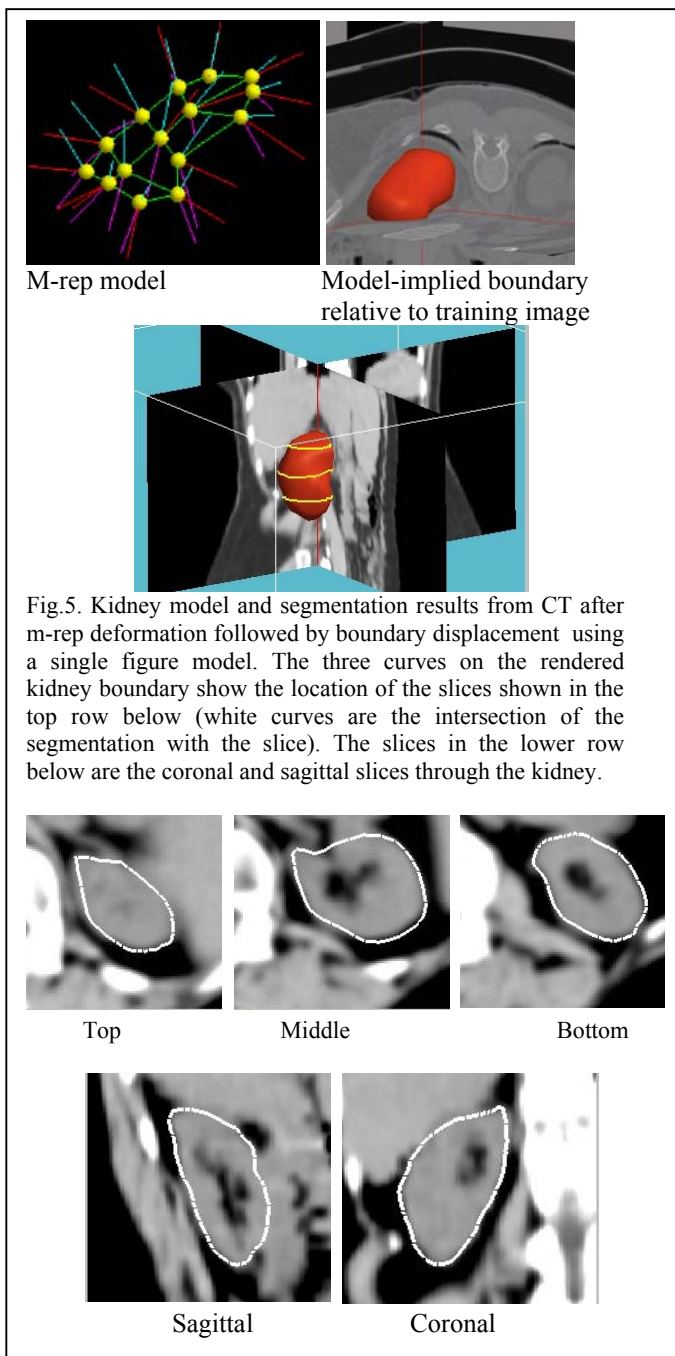


Fig.5. Kidney model and segmentation results from CT after m-rep deformation followed by boundary displacement using a single figure model. The three curves on the rendered kidney boundary show the location of the slices shown in the top row below (white curves are the intersection of the segmentation with the slice). The slices in the lower row below are the coronal and sagittal slices through the kidney.

Thus, we take the success of this segmentation method as evidence for the object-intrinsic correspondences on which both its geometric typicality measurement and its geometry-to-image match measurement are based. Moreover, these correspondences will also allow the improvement of the method by replacing the present measures by Bayesian, statistical log probability measures, founded on statistical characterizations that depend on the object-intrinsic

homology. Such statistical characterization of geometry is discussed in section B, which follows immediately.

B. Statistical object class characterization via intrinsic coordinates

In-vivo imaging studies of brain structures have examined disorders including neurodegenerative diseases and/or disorders of abnormal neurodevelopment. Driving clinical applications in our lab are neuroimaging studies of subcortical structures in schizophrenia, autism, and epilepsy. Structural imaging studies have so far most often focused on volumetric assessment of gross brain structures. With increasing evidence for structural changes in small subregions and parts of structures and the availability of improved three-dimensional imaging techniques, there is a need for providing new image analysis techniques suitable for these tasks. For example, earlier studies of whole ventricular volumes have to be replaced by subfigural shape studies of parts of ventricles, and there is even evidence that regional shape analysis of the hippocampus structure could differentiate schizophrenics from controls whereas volume differences are not significant. Improved global and local structure characterization might help to explain pathological changes in neurodevelopment / neurodegeneration in terms of their biological meaning.

The specific applications for which we give results below are the detection of group differences of amygdala-hippocampal shapes in schizophrenia and the analysis of ventricular shape similarity in a mono/dizygotic twin study. These support our hypothesis that shape captures information on structural similarity or difference that is not accessible by volume analysis and that the intrinsic coordinates provided by m-reps provide the sensitivity, locality, and intuitiveness of results needed by neuroscientists.

Statistical studies of the shape of anatomical structures requires models fitted for statistical analysis. That is, the geometric models themselves must be built to be suitable for the description of whole populations of example structures. The method devised by Styner is described in [Styner 2001b]. Beginning with experts' segmentation of dozens of training images, the pipeline involves intermediate spherical harmonic (SPHARM) descriptions [Brechtbühler 1995, Székely 1996, Kelemen 1999] and point distribution models [Cootes 1995, Styner 2001b] as well as Voronoi medial axes [Naef 1996]. The pipeline determines the common topology of the skeleton that represents each individual shape up to a predefined approximation error and then the m-rep grid sampling that guarantees meeting a threshold of boundary location error for all objects in the statistical shape class and for a rather dense sample of the (u,v,t) intrinsic coordinates of the boundary. The medial atoms of the m-rep become the random variables for the statistical study to follow.

Shape analysis has so far been applied to several clinical studies with several hundreds of anatomical objects. In all of these studies, anatomical objects for each group (e.g., healthy controls and schizophrenics) were segmented by automatic, model-based SPHARM segmentation [Kelemen 1999] or by manual expert's contour drawing. The m-rep models for each brain shape were calculated using the described automatic model-building framework, where global shape alignment is

solved by Procrustes fit of homologous surfaces [Styner 2001a,b, 2002, Gerig 2001a]. Deformable m-rep segmentation for various brain structures will soon replace the time-consuming and tedious manual segmentation step. Right brain objects were flipped at the symmetry plane for joint analysis or analysis of asymmetry. The m-rep model fitting results in a homology of mesh medial atoms between left/right pairs but also among all shapes, which is used for both integrated global shape comparison and also local analysis.

In the statistical analysis, radius and m-rep atom location was used to calculate local and global measures of radius difference (mean absolute difference of radii) and medial mesh deformation (Euclidean distance between corresponding mesh nodes' medial positions). These shape difference measures were calculated for pairs in each group or as differences from the overall average shapes. Finally, we used standard statistical mean difference tests to determine significance of global and local shape differences.

A.1. Amygdala-hippocampal shape asymmetry in schizophrenia

In a collaborative study with the Brigham and Women's Hospital, Harvard [Shenton 2002], we studied hippocampal shape changes and asymmetry as a group comparison between healthy controls (N=15) and schizophrenics (N=15). Earlier findings demonstrated significant volume asymmetry of the hippocampus but not the amygdala hippocampal complex. Our results (Fig. 6) showed that neither shape asymmetry nor volume asymmetry was significant, but in the joint analysis using multivariate statistics [Gerig 2001b] a shape asymmetry was found. The major asymmetry was in the hippocampal tail. M-rep analysis nicely showed the type of shape difference, which was increased bending of the tail of the right hippocampal shape but not change of local width.

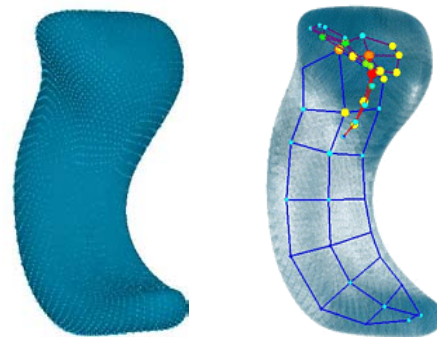


Fig. 6. Average amygdala-hippocampus shape (left) and M-rep model. The size of the balls and their color represent the local width.

A.2. Lateral ventricle shape in twin studies

Imaging studies of twins are becoming increasingly important to study the genetic factor of shape variability in healthy control populations but also to understand disease through identical twins discordant for disease (one twin subject diagnosed with disease, the paired twin not diagnosed but considered as a subject at risk). In close collaboration with a research group at NIMH (Daniel Weinberger), we

segmented brain images of 40 twin pair datasets, with 20 identical healthy controls, 20 non-identical healthy controls, and 20 identical subjects discordant for schizophrenia. Lateral ventricles were segmented by manually editing tissue classification maps, and m-rep representations were obtained using the procedure as outlined above [Gerig 2001a, Styner 2001a,b, 2002]. Pairwise shape differences (bottom Fig. 7) of left and right ventricles were measured for identical twin pairs, non-identical twin pairs, nonrelated subjects, and the identical discordant pairs. M-rep shape analysis results in integrated and local measures of absolute radius difference (growth parameter) and of mesh deformation (bending). Results of the complete study are not yet published, but early tests show a significantly higher shape similarity of identical twin pairs in comparison to non-identical pairs, suggesting a genetic influence on the ventricle shape. However, this similarity was only significant after shapes were uniformly scaled by individual volumes, which raises important questions for future studies in regard to a task-dependent choice of size normalization.

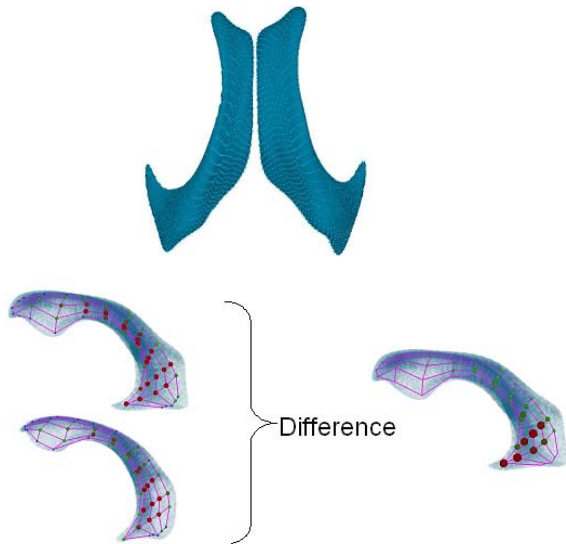


Fig. 7. Shape comparison of ventricle shape in twin pairs: Top view of lateral ventricles (left), side views of right ventricles of twin A and twin B (middle), and difference of right ventricles between twin A and B. Width differences at homologous m-rep atom locations are shown with spheres of varying radius and clearly show the major difference in the atrium region of ventricles.

A.3. Hippocampal shape change in schizophrenia

The hippocampus is a structure of major interest in many brain diseases and mental illness, e.g. epilepsy, Alzheimer's disease, and schizophrenia. Current studies redirect the focus from volumetric measurements to localized assessment of hippocampal shape changes [Csernansky 1998]. In a most recent clinical study at UNC, we segmented the hippocampal structure in a control population (N=30) and a schizophrenic population undergoing different type of drug treat-met (N=60). M-reps of the 90 left and right hippocampal shapes were obtained using the procedure outlined above. Statistical

group tests (Fig. 8) were calculated on integrated whole structure measurements and on local measurements at each medial atom for both difference in width (growth) and difference in mesh location (bending). Early results indicate that the major shape effect is found in the bending of hippocampal tail but not a width difference in the same region. This finding underlines the increased power of the m-rep representation versus conventional surface description of shape changes, as shape changes can be expressed by a quantitative, intuitive description rather than 3D color graphics representation.

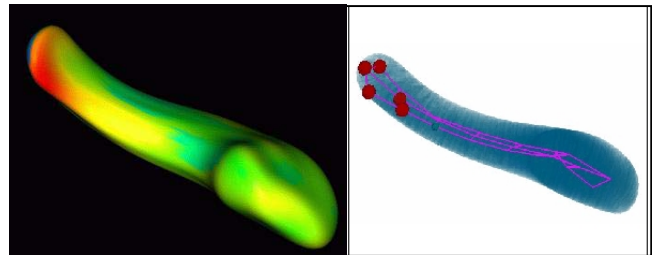


Fig. 8. Shape analysis of hippocampus structure in a control / schizophrenics study. Left: Surface display of the difference between group mean shapes with color-coded regions of major change (red: outwards, blue: inwards). Right: Local statistical analysis of m-rep representations presenting significant locations of grid deformation. The locations of significance difference are shown as red balls.

The usefulness and success of these studies requiring statistical characterization of populations of objects and discrimination of the populations by their geometry depend on the intrinsic coordinates given by m-reps. They thus provide further evidence for the usefulness of these particular object-intrinsic coordinates.

VI. DISCUSSION AND FUTURE PLANS

A popular method for finding correspondence between anatomical images uses landmark-based transformations, computed from groups of manually chosen landmarks that have been statistically analyzed [Dryden 1998, Luo 1999]. These methods operate at a large scale only and provide global shape information.

Another popular method for finding correspondence between anatomical images uses a registration transformation that maps the underlying coordinate system of an atlas image to the set of images under study to produce a diffeomorphic transformation $h(x)$ mapping the coordinate systems of the different images, i.e., a correspondence [Yuille 1991, Christensen 1997, Joshi 2000]. The transformation is computed via an energy minimization with the energy being a sum of an image similarity measure and a regularization term, which constrains the transformation to be diffeomorphic. The regularization energetic in form of differential operator norms are usually motivated by continuum mechanical models. In this framework the underlying space is modeled either as elastic or a fluid medium. Although these methods provide a correspondence, they are not based on the intrinsic geometry of the constituent objects. One of the most promising

extensions suggested to the registration methods is to derive the regularization energetics from a model-based statistical analysis of a sample set of registration maps [Grenander 1998].

Object boundary points have provided a geometric means for producing correspondences to be used to obtain statistics of geometry. These diffeomorphisms are provided by global analysis of the boundary, e.g., via Active Shape Models via point distribution representations [Cootes 1995, Wang 1998], via spherical harmonics [Kelemen 1999], and via meshes [Pentland 1991, Martin 1998, Delingette 1999].

M-reps also provide a geometric means for producing correspondences, but unlike boundary-based methods they give advantages of locality and a natural multiscale sequence, and they give correspondences in the whole interior and nearby exterior of an object and not just on the boundary. Moreover, they give correspondences in orientation and in a distance metric across instances of an object.

Among the limitations of medially based coordinate systems is their sensitivity in the case that the object is nearly circularly symmetric in one or two of the medial dimensions. That is, there are problems with nearly tubular structures, with near-pancakes, and with near-spheres. This is an inherent problem of objects with symmetries, not a problem related to a particular means of representation.

We are working on unifying the m-rep based geometrical correspondence with the correspondences of a variety of geometric features learned through statistics. These features can result from geometric analysis in figural coordinates, e.g., of boundary bumps and nearby objects' crests, and they can be defined using the energetic regularizing the registration transformation. The resulting small scale variations in correspondence can be represented by diffeomorphisms of the (u, v) figural coordinates.

A. Future plans for segmentation

The deformable m-reps method described here is by no means fully developed. The metrics, the segmentation algorithm, and the visualizations have already been extended to deal with objects made up of multiple attached figures which must be kept in the correct geometric relations as they deform. Examples are the cerebral ventricle, the vertebra, and the kidney subdivided into parenchyma and renal pelvis. Extension has also been made to deal with multiple nonoverlapping figures which must be kept in the right geometric relations and to remain noninterpenetrating. Examples are the pubic bones, bladder, prostate, and rectum in the male pelvis and the full set of cerebral ventricles. Early, incomplete trials of the extended versions of the code suggest that m-reps have particular advantages also with multiple attached figures and multiple nonoverlapping figures [Fletcher 2000].

The replacement of the geometric distance measures for geometric typicality and average intensity correlation for the geometry-to-image match measure by log probability measures [Cootes 1999] has two important advantages. First, the probabilities reflect the modes of variability in the respective population. Second, the arbitrary, manually selected weight between geometric typicality and geometry to

image match is no longer necessary. We have begun work on methods for measuring these probabilities from training sets, at each of the relevant scale levels based on a Markov random field model, and for using them in the model deformation process.

B. Future plans for shape studies

Current studies clearly show a need for studying groups of anatomical object in combination rather than describing their shapes independently. Multi-object extension of the m-rep method will be applied for the hippocampus/ amygdala and caudate/ventricle objects as part of the prefrontal cortical-hippocampal network. The increased sensitivity of the new tools has the potential of detecting brain structure differences between different forms of brain disease (neurodevelopmental and neurodegenerative) and even subtle changes within patients over the course of their illness. This will reveal a new insight into shape abnormalities of brain structures specific to schizophrenia, via exploring shape variations, anomalies and asymmetries in well-defined patient and control groups.

C. Conclusion

We have argued and provided evidence that image analysis, especially image analysis via generative statistical models, depends strongly on good correspondences between positions, orientations, and metrics across members of the object population. We have found that the correspondences provided via the object representations given by m-reps have peculiar advantages in this regard and lead to successes in 3D object segmentation and in statistical discriminations of geometric properties between populations of 3D objects.

ACKNOWLEDGEMENTS

We are grateful to conceptual, geometric, algorithmic, or code contributions from Graham Gash and Guodong Liu. We thank Edward Chaney and Gregg Tracton for providing driving problems for this segmentation, images to segment, and segmentations and Delphine Bull and James Chen for help with this manuscript. Paul Yushkevich helped to develop ideas on multiscale residues. This work was done under the partial support of NCI Grant P01 CA47982, NSF grant CCR SGER 9910419, Stanley Foundation and the UNC-MHNCRC (MH33127).

REFERENCES

- Blum, H, RN Nagel (1978). Shape description using weighted symmetric axis features. *Pattern Recognition* **10**:167-180.
- Brechtbuehler, Ch, G Gerig, O Kuebler (1995). Parametrization of closed surfaces for 3D shape description. *Comp. Vision and Image Underst.*, **61**(2):154-170.
- Christensen, GE, SC Joshi, and MI Miller (1997). Volumetric transformation of brain anatomy. *IEEE Transactions on Medical Imaging*, **16**(6):864-877.
- Cootes, TF, CJ Taylor, DH Cooper, J Graham (1995). Active shape models - their training and application. *Computer Vision and Image Understanding*, **61**(1):31-59.
- Cootes, T and Taylor A (1999). Unified framework for atlas matching using active appearance models. IPMI 1999, **1613**: 322-333.
- Crouch, JR, SM Pizer, EL Chaney, M Zaider (2001). Elastic registration of prostate images using the finite element method with m-rep models. Poster, 2nd Int. Conf. On Innovative Solutions for Prostate Cancer Care. Also at website www.cs.unc.edu/Research/Image/MIDAG/pubs/presentations/prostate-mrep-Crouch2001_files/frame.htm.
- Csernansky, J, S Joshi, L Wang, J Haller, M Gado., J Miller, U Grenander, M Miller (1998). Hippocampal morphometry in schizophrenia via high dimensional brain mapping. *Proc. Natl. Acad. Sci. USA*, **95**:11406-11411.
- Damon, J (2002). Smoothness and geometry of boundaries associated to skeletal structures. Internal report, Dept. of Mathematics, Univ. of NC.
- Delingette, H (1999). General object reconstruction based on simplex meshes. *International Journal of Computer Vision*, **32**:111-146.
- Dryden, IL, KV Mardia (1998). *Statistical Shape Analysis*. John Wiley and Sons (Chichester).
- Fletcher, PT, SM Pizer, AG Gash, S Joshi (2002). Deformable m-rep segmentation of object complexes. Proc. IEEE International Symposium on Biomedical Imaging.
- Gerig, G, M Styner, D Jones, D Weinberger, JA Lieberman (2001a). Shape analysis of brain ventricles using SPHARM. Proc. Mathematical Methods in Biomedical Image Analysis (MMBIA 2001), IEEE Computer Society: 171-178.
- Gerig, G, M Styner, ME Shenton, JA Lieberman (2001b). Shape versus size: improved understanding of the morphology of brain structures, Proc. MICCAI 2001, Springer LNCS **2208**: 24-32.
- Grenander, U, MI Miller (1998). Computational anatomy: an emerging discipline. *Quarterly of Applied Math.*, **56**: 617-694.
- Joshi, S, MI Miller (2000). Landmark matching via large deformation diffeomorphisms. *IEEE Transactions on Image Processing*, **9**(8):1357-1370.
- Joshi, S, SM Pizer, PT Fletcher, A Thall, G Tracton (2001). Multi-scale 3-D deformable model segmentation based on medical description. Proc. IPMI 2001, **2082**:64-77.
- Kelemen, A, G Szekeley, G Gerig (1999). Elastic model-based segmentation of 3D neuroradiological data sets. *IEEE Transactions On Medical Imaging*, **18**: 828-839.
- Luo, B, ER Hancock (1999). Matching point-sets using Procrustes alignment and the EM algorithm. Proc. British Mach. Vis. Conf : 43-52.
- Martin, J, A Pentland, S Sclaroff, R Kikinis (1998). Characterization of neuropathological shape deformations. *IEEE Trans. Pattern Analysis and Machine Intelligence* **20**: 97-112 .
- Naef, M, O Kuebler, R Kikinis, M Shenton, G Szekeley (1996). Characterization and recognition of 2D organ shape in medical image analysis using skeletonization. Proc. of IEEE Workshop on Mathematical Methods in Biomedical Image Analysis (MMBIA 1996): 139-150.
- Pentland, A, S. Sclaroff (1991). Closed-form solutions for physically based shape modeling and recognition. *IEEE Trans. Pattern Analysis and Machine Intelligence*, **13**: 715-729.
- Pizer, SM, JZ Chen, PT Fletcher, Y Fridman, D Fritsch, AG Gash, J Glotzer. MR Jiroutek, S Joshi, KE Muller, A Thall, G Tracton, P Yushkevich, EL Chaney (2002). Deformable m-reps for 3D medical image segmentation. Submitted, at website <http://midag.cs.unc.edu/pubs/papers/IJCV01-Pizer-mreps.pdf>.
- Shenton, ME, G Gerig, RW McCarley, G Szekeley, R Kikinis (2002). Amygdala-hippocampus shape differences in schizophrenia: the application of 3D shape models to volumetric MR data. *Psychiatry Research Neuroimaging*, to appear.
- Styner, M, G Gerig (2001a). Medical models incorporating object variability for 3D shape analysis. Proc. IPMI 2001, **2082**: 502-516.
- Styner, M, G Gerig (2001b). Three-dimensional medial shape representation incorporating object variability. Proc. Computer Vision and Pattern Recognition (CVPR 2001), *IEEE Computer Society*: 651-656.
- Styner, M, G Gerig, SM Pizer, S Joshi (2002). Automatic and robust computation of 3D medial models incorporating object variability, to appear, *IJCV*.
- Székeley, G, A Kelemen, C Brechtbühler, G Gerig (1996). Segmentation of 2-D and 3-D objects from MRI volume data using constrained elastic deformations of flexible Fourier contour and surface models. *Medical Image Analysis* **1**(1): 19-34.
- Thall, A (2002). Fast C^2 interpolating subdivision surfaces using iterative inversion of stationary subdivision rules. University of North Carolina Computer Science Department technical report TR02-001.
- Willis, LA (2001). Geometric description of lung shape during respiration via m-reps and normalized mutual information. MS thesis 2001, Dept. of Biomedical Engineering, UNC in preparation.
- Yuille, A (1991). Deformable templates for face recognition. *J. Cognitive Neuroscience* **3**(1).
- Yushkevich, P, SM Pizer, S Joshi, JS Marron (2001). Intuitive, localized analysis of shape variability. Proc. IPMI 2001, **2082**: 402-408.
- Wang, Y, LH Staib (1998). Boundary finding with correspondence using statistical shape models. Proc. Conf. Computer Vision and Pattern Recognition: 338-345.